


Collective Dynamical Fermi Suppression of Optically Induced Inelastic Scattering

Camen A. Royse, J. Huang[✉], and J. E. Thomas^{✉*}*Department of Physics, North Carolina State University, Raleigh, North Carolina 27695, USA* (Received 26 January 2024; revised 17 April 2024; accepted 27 June 2024; published 20 August 2024)

We observe strong dynamical suppression of optically induced loss in a weakly interacting Fermi gas as the s -wave scattering length is increased. A single trapped cigar-shaped cloud behaves as a large spin lattice in energy space with a tunable Heisenberg Hamiltonian. The loss suppression occurs as the lattice transitions into a magnetized state, where the fermionic nature of the atoms inhibits interactions. The data are quantitatively explained by incorporating spin-dependent loss into a quasiclassical collective spin vector model, the success of which enables the application of optical control of effective long-range interactions to this system.

DOI: 10.1103/PhysRevLett.133.083404

In trapped, ultracold gases, understanding optically induced atom loss is essential for developing optical probes and control methods for many-body systems [1–5]. Loss due to optically induced inelastic scattering has been used to study the BEC-BCS crossover in a Fermi gas via photoassociation [6] and accompanies optical control of the s -wave scattering length [7–11]. Modeling optically induced two-body loss in a coherently prepared, weakly interacting Fermi gas is nontrivial, as it exhibits a coherent many-body spin evolution [12–20]. Understanding this loss allows the spin dynamics to be probed and enables optical control of interactions in this system, which can be used to engineer the Hamiltonian [21].

The Pauli principle plays an essential role in the evolution of the loss in an ultracold, weakly interacting Fermi gas, as the atoms cannot undergo inelastic s -wave scattering when the spin state of a colliding atom pair is symmetric. This is especially relevant when the gas evolves into a magnetized state, which occurs at a sufficiently large scattering length [18,22]. Fermi gases have recently provided new demonstrations of the Pauli principle in degenerate samples, where Pauli blocking suppresses light scattering for atoms in a Fermi sea [23–26]. In contrast, the suppression of light scattering reported here emerges from effective long-range spin-spin interactions and is both dynamical and collective.

In this Letter, we examine the collective suppression of optically induced inelastic scattering in a weakly interacting ^6Li Fermi gas. Each atom is prepared in a pseudospin-state comprising a superposition of the two lowest hyperfine states $|1\rangle$ and $|2\rangle$. As the s -wave scattering length is increased, we observe a crossover from high to low optically induced loss. We develop and test a model for

the spin-dependent loss, which shows that dynamical loss suppression arises from the onset of a magnetized state.

Tunable two-body scattering with optically induced loss is accomplished using a collisional Fano-Feshbach resonance, Fig. 1(b). The resonance arises from hyperfine coupling between the triplet $^3\Sigma_u$ continuum $|k\rangle$ and a molecular vibrational state $|g_1\rangle$ in the singlet $^1\Sigma_g$ channel. At low temperatures, where s -wave scattering dominates, the s -wave scattering length a_s is controlled by a bias magnetic field B_z , which tunes the total Zeeman-hyperfine energy of an incoming pair of atoms in state $|k\rangle$ near

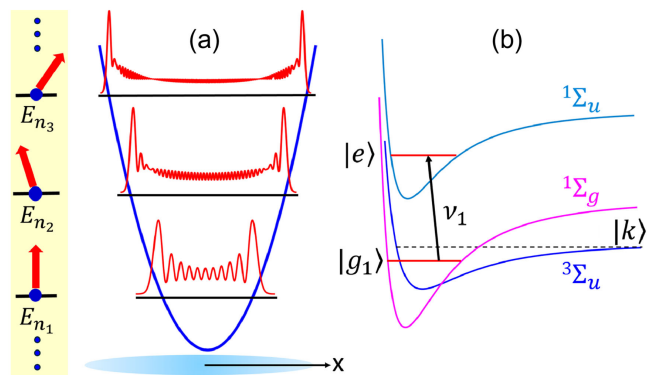


FIG. 1. (a) Energy-space spin lattice. Atoms remain fixed at axial energy “sites” ($0 \leq n \lesssim 650$) in the harmonic potential of a cigar-shaped optical trap. Collective spin vectors (large red arrows) in each axial x energy state E_n contain pseudospins in several transverse (y, z) states. Site-to-site couplings $n \leftrightarrow n'$ are determined by the overlap of the spatial probability distributions $|\phi_n(x)|^2$. (b) Molecular states for two-body scattering near a Fano-Feshbach resonance. A pair of atoms collides in a relative momentum state $|k\rangle$ in the triplet channel $^3\Sigma_u$, which is hyperfine-coupled to a bound state $|g_1\rangle$ in the singlet channel $^1\Sigma_g$. Loss is induced by an optical field ν_1 that drives a transition from $|g_1\rangle$ to $|e\rangle$.

*Contact author: jethoma7@ncsu.edu

resonance with $|g_1\rangle$. Inelastic loss is induced by an optical field ν_1 resonant with a transition from $|g_1\rangle$ to an excited electronic state $|e\rangle$, which spontaneously decays, causing loss of both atoms from the trap [8,11,27]. Related level schemes have been used for optical control of a_S via a ν_1 -induced light shift of $|g_1\rangle$ [7,8,10,11]. As the s -wave relative motion state is symmetric under the interchange of the atom labels, denoted i, j , scattering in the Fermi gas requires an antisymmetric two-atom hyperfine state, $|\Psi_a(i, j)\rangle = (1/\sqrt{2})(|1\rangle_i|2\rangle_j - |2\rangle_i|1\rangle_j)$. Hence, the projection of the two-atom pseudospin state onto $|\Psi_a(i, j)\rangle$ determines the scattering probability.

A “weakly interacting” Fermi gas is created by tuning a_S to be small enough that the energy-changing collision rate $\propto a_S^2$ is negligible during each measurement period. In the absence of optically induced loss, atoms remain fixed in their respective energy states, allowing the system to be described as a lattice in a “synthetic dimension” [28] formed by the energy eigenstates of the trapping potential, Fig. 1(a). The lattice picture simplifies the description in comparison to a real space treatment, as the motional states of the atoms are fixed and the system evolves via pure spin dynamics, simulating a collective Heisenberg Hamiltonian [12–20]. We will use the word “site” or “energy site” to denote the “location” n of an energy group in the synthetic lattice.

In our experiments, the atoms are confined in a cigar-shaped optical trap. The curvature of a bias magnetic field $\partial_x^2 B_z$ along the cigar axis x produces a precession rate $\Omega'_x E$ for pseudospins of axial energy E [21]. Because of the tight transverse confinement, Ω'_y and Ω'_z are 900 times smaller than Ω'_x and negligible. This allows a 1D approximation for the lattice, where the dependence of the spin-spin couplings on the different transverse states is replaced by a transverse probability density-averaged coupling. Then, all pseudospins in a group with nearly the same axial energy E evolve in the same way, as described by a *collective* spin vector $\mathbf{S}(E, t)$ for each site. We find that this model is in very good agreement with our observations [14,21,22,29].

Without loss, the evolution of $\mathbf{S}(E, t)$ is described by the spin Hamiltonian $H(E) = \boldsymbol{\omega}(E) \cdot \mathbf{S}(E)$, where

$$\boldsymbol{\omega}(E) = \Omega'_x E \hat{\mathbf{e}}_z + \sum_{E' \neq E} g(E, E') \mathbf{S}(E'). \quad (1)$$

Here, $g(E, E') \propto a_S$ is the coupling between spins at axial energy sites E and $E' \neq E$, which is proportional to the overlap of the spatial probability densities, producing effective long-range interactions. The coupling arises from forward scattering between atoms in two different spin states, where the identical spin rotation effect (ISRE) [17,30,31] causes a rotation of each spin about the conserved total spin vector. In our experiments, for $a_S = 5.0a_0$ with a_0 the Bohr radius, the average coupling $\bar{g} \simeq 1.6 \text{ Hz} \times 2\pi$. The rms spread in $\Omega'_x E$, denoted $\Omega'_x \sigma_E$, is $\simeq 1.4 \text{ Hz} \times 2\pi$. Defining $\mathbf{S}(E, t) = S(E, t) \hat{\mathbf{S}}(E, t)$, where $\hat{\mathbf{S}}(E, t)$ is a unit vector,

$$\dot{\mathbf{S}}(E) = S(E) \dot{\hat{\mathbf{S}}}(E) + \dot{S}(E) \hat{\mathbf{S}}(E). \quad (2)$$

Here $S(E, t) = N_E(t)/2$ with $N_E(t)$ the number of atoms with axial energy E . Neglecting loss, where $\dot{S}(E) = 0$, the rotation of $\mathbf{S}(E)$, given by the first term in Eq. (2), is determined by the Heisenberg equations,

$$\dot{\hat{\mathbf{S}}}(E, t) = \boldsymbol{\omega}(E, t) \times \hat{\mathbf{S}}(E, t). \quad (3)$$

We solve Eq. (3) for the unit vectors $\hat{\mathbf{S}}(E, t)$ in a quasiclassical approximation, treating $\mathbf{S}(E, t)$ and $\mathbf{S}(E', t)$ as classical vectors.

The evolution of the collective spin vectors is determined by the competition between $\boldsymbol{\Omega}_B(E) \equiv \Omega'_x E \hat{\mathbf{e}}_z$ and $\boldsymbol{\omega}_{MF}(E, t) \equiv \sum_{E' \neq E} g(E, E') \mathbf{S}(E', t)$ in Eq. (1). As the lattice is not in thermal equilibrium, this competition results in two *dynamical* phases: a spin-unlocked phase, where $\boldsymbol{\Omega}_B(E)$ dominates and a spin-locked phase, where $\boldsymbol{\omega}_{MF}(E, t) \propto a_S$ dominates, independent of the sign of a_S . With increasing $|a_S|$, the lattice exhibits a crossover between these two dynamical phases [18,22]. As the pseudospins are initially spin polarized, they cannot interact until $\boldsymbol{\Omega}_B(E)$ causes the collective spin vectors to fan out with E -dependent angles in the transverse plane. The crossover is characterized by the interaction strength $\zeta \equiv \bar{g}/(\Omega'_x \sigma_E \sqrt{2})$ [21,22]. For small a_S , ζ is small and $\boldsymbol{\Omega}_B(E)$ dominates, which is reflected in a low magnitude of the total spin vector $S(t) = |\sum_E \mathbf{S}(E, t)|$, Fig. 2. We find that when a_S is large enough that $\zeta \gtrsim 1.5$, $\boldsymbol{\omega}_{MF}(E, t)$ dominates over $\boldsymbol{\Omega}_B(E)$ and the spins lock together. However, spin locking produces parallel spins that suppress the spin-rotation rate $\propto \mathbf{S}(E) \times \mathbf{S}(E')$, enabling $\boldsymbol{\omega}_B(E)$ to again fan

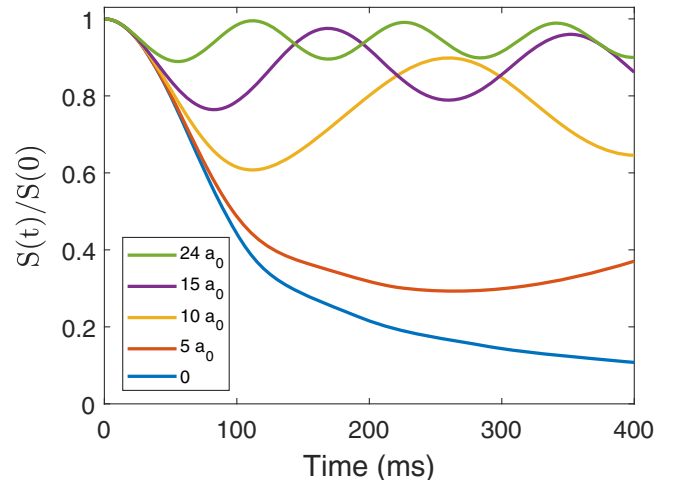


FIG. 2. Predicted magnitude of the total spin vector as a function of time for loss-free evolution with different s -wave scattering lengths. In the model, we use the experimental parameters given in the text. For $a_S/a_0 = 0, 5, 10, 15, 24$ (bottom to top), the respective interaction strengths are $\zeta = 0, 0.8, 1.6, 2.4, 3.9$.

out the spin vectors, which then reenables scattering and subsequent spin locking, resulting in an oscillation of $S(t)$, Fig. 2. With increasing $\zeta \propto |a_S|$, the average $S(t)$ (magnetization) increases and the oscillation amplitude decreases.

Inelastic scattering is optically induced as described above, Fig. 1(b). Spontaneous emission from $|e\rangle$ causes loss of both atoms, without heating or pumping into higher- or lower-energy trap modes, allowing use of the energy-space spin-lattice picture. With loss, the collective spin vectors rotate and change length, Eq. (2) with $\dot{S}(E, t) = \dot{N}_E(t)/2 \neq 0$. To incorporate loss into the model, we determine $N_E(t)$ as follows.

Loss due to two-body inelastic collisions between two species A and B with 3D densities $n_A(\mathbf{r}, t)$ and $n_B(\mathbf{r}, t)$ is generally modeled as

$$\dot{n}_A(\mathbf{r}, t) = \dot{n}_B(\mathbf{r}, t) = -K_2^{AB} n_A(\mathbf{r}, t) n_B(\mathbf{r}, t). \quad (4)$$

Here $K_2^{AB} \equiv \langle v_r \sigma_{\text{inel}}^{AB} \rangle$ with $\sigma_{\text{inel}}^{AB}$ the AB inelastic cross section and $\langle \dots \rangle$ denotes an average over relative speed v_r . In the energy-space spin lattice, each energy corresponds to a definite spin vector. In our quasiclassical picture, atoms of axial energy E , in the spin state $|\hat{S}(E)\rangle$, collide with atoms of energy E' in the spin state $|\hat{S}(E')\rangle$ for all $E' \neq E$. To find $N_E(t)$, we generalize Eq. (4) to model the loss of the spin-energy correlated 3D densities $n_E(\mathbf{r}, t)$, i.e., the density of atoms with axial energy E :

$$\dot{n}_E(\mathbf{r}, t) = - \sum_{E'} K(E, E', t) n_E(\mathbf{r}, t) n_{E'}(\mathbf{r}, t), \quad (5)$$

where $K(E, E', t)$ is the effective loss rate coefficient. Spin-dependent Fermi suppression is manifested in our expression for $K(E, E', t)$, which weights the two-body loss coefficient K_2^a associated with the *antisymmetric* two-atom hyperfine $|\Psi_a(i, j)\rangle$ by the probability that the incoming two-atom spin state $|\hat{S}(E)\rangle_i |\hat{S}(E')\rangle_j$ is in the state $|\Psi_a(i, j)\rangle$ [21],

$$K(E, E', t) = \frac{K_2^a}{4} [1 - \hat{S}(E, t) \cdot \hat{S}(E', t)]. \quad (6)$$

In the quasiclassical approximation, dynamical suppression of loss appears in the time dependence of the unit vectors, $\hat{S}(E, t)$. $K(E, E', t)$ has a maximum of $K_2^a/2$ when the colliding spin vectors are antiparallel and vanishes when the spin vectors are parallel, which is most likely for a magnetized state.

To determine $N_E(t)$ from Eq. (5), we employ a quasi-1D approximation, where the 3D density factors [21]: $n_E(\mathbf{r}, t) = n_E(\rho, x, t) \simeq N_E(t) \mathcal{R}(\rho, t) |\phi_E(x)|^2$. Here x is the axial coordinate and ρ is the radial coordinate. We take $\mathcal{R}(\rho, t)$ to be the normalized transverse probability density, $\int d\rho 2\pi\rho \mathcal{R}(\rho, t) = 1$ for all t and $\int d^3\mathbf{r} n_E(\mathbf{r}, t) = N_E(t)$. Integrals of Eq. (5) over x, ρ result in coupled

equations for $\dot{\mathcal{R}}(\rho, t)$ and $\dot{N}_E(t)$ [21]. Density-dependent loss causes $N_E(t)$ to decrease in time and $\mathcal{R}(\rho, t)$ to change shape, reducing the average transverse probability density $\bar{n}_\perp(t) = \int d\rho 2\pi\rho [\mathcal{R}(\rho, t)]^2$. While we cannot directly measure $\mathcal{R}(\rho, t)$, including the time dependence of $\bar{n}_\perp(t)$ is essential, as is made apparent by comparing the measured loss rates to the model predictions with $\bar{n}_\perp = \bar{n}_\perp(t)$ and with $\bar{n}_\perp = \bar{n}_\perp(0)$ [21]. The evolution equations for $S(E, t) = N_E(t)/2$, $\hat{S}(E, t)$, and $\mathcal{R}(\rho, t)$ determine the evolution of the total atom number $N(t) = \sum_E N_E(t)$.

To test the loss model, we measure the time-dependent loss of the total atom number $N(t)$ for scattering lengths $a_S = 0$ to 24 Bohr (a_0), corresponding to interaction strengths $\zeta = 0$ to 5.39. The trapped gas is illuminated by a nominally uniform optical field resonant with the $|g_1\rangle \rightarrow |e\rangle$ transition and evolves for a variable amount of time before resonant absorption imaging of the atom densities for the spectrally resolved hyperfine states $|1\rangle$ and $|2\rangle$.

In the experiments, a gas of $N(0) = 6 \times 10^4$ ^6Li atoms is prepared in the weakly interacting regime [14]. The temperature of the gas is $T = 0.18T_F$, where the Fermi temperature $T_F \simeq 0.75$ μK . We use the calibration from Ref. [14] to tune to the desired scattering length $a_S(B)$, where rf spectroscopy precisely determines B . A 0.5 ms $\pi/2$ RF pulse is applied to a z -polarized sample to prepare the atoms in an equal superposition of the lowest-energy hyperfine states $|1\rangle$ and $|2\rangle$, i.e., the pseudospins are initially polarized orthogonal to the magnetic field direction z . Immediately following the pulse, a loss-inducing optical field is applied and the system evolves for a time $0 \leq t \leq 400$ ms. The Rabi frequency of the optical field is estimated to be [21] $\Omega_1 \simeq \gamma_e/2$, where $\gamma_e = 2\pi \times 11.8$ MHz is the spontaneous emission rate from the excited molecular state $|e\rangle$. Since the optical field is on resonance, there is no optical shift of the scattering length [27]. The trap frequencies are $\omega_\rho = 2\pi \times 668$ and $\omega_x = 2\pi \times 25$ Hz. A fit to a zero-temperature Thomas-Fermi profile yields an axial width $\sigma_{TF} = 330$ μm . The radial width of 12 μm is computed from the ratio of the trap frequencies. For each measurement with a coherently prepared sample, the two-body loss rate coefficient K_2^a is measured for a 50-50 mixture. These measured values of K_2^a are used as inputs into the loss model.

The fraction of atoms remaining after 370 ms of illumination, $N(370 \text{ ms})/N(0)$, is shown in Fig. 3 for the different scattering lengths. The data demonstrate a crossover between the unlocked and spin-locked dynamical phases, where the Fermi suppression more than doubles the number of atoms remaining between the $a_S = 0$ and 24 a_0 cases. Error bars represent the standard deviation of the mean for six shots. The prediction generated by the loss model (red curve) agrees well with the data. For the prediction, we use the averaged atom number, axial widths, and values of K_2^a from the measurements.

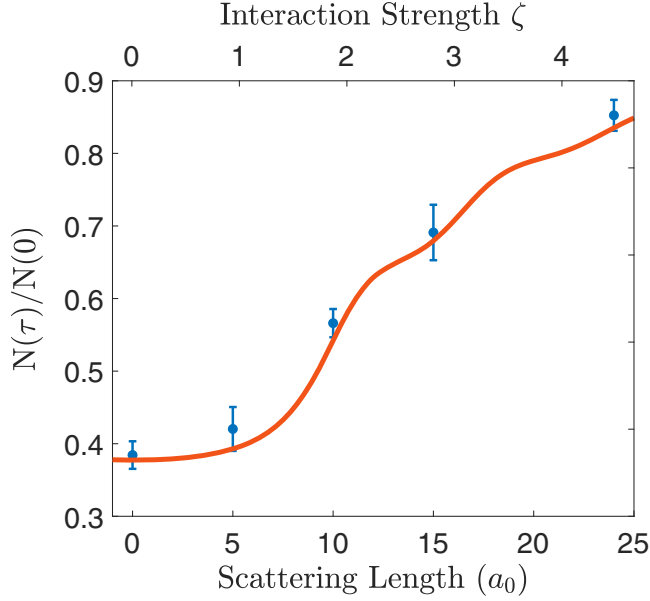


FIG. 3. Measurements of the atom fraction remaining after $\tau = 370$ ms of illumination (blue points) vs scattering length and interaction strength ζ , compared to the theoretical prediction (red curve). The densities and values of K_2^a vary slightly for each measurement [21]. For the prediction, we use the average values $N(0) = 6.1 \times 10^4$ atoms, $\sigma_{TF} = 332 \mu\text{m}$, and $K_2^a = 62 \mu\text{m}^3/\text{s}$.

Measurements of the fraction of atoms remaining throughout the evolution $N(t)/N(0)$ for coherently prepared samples are shown in Fig. 4, along with the corresponding predictions using no free parameters. Predictions and measurements for $a_S = 0a_0$ ($\zeta = 0$), where

interactions are absent, are shown as a reference, and agree very well. The atom number is nearly stagnant for the first ≈ 80 ms, corresponding to the time needed for the energy-dependent Zeeman precession rates to separate the collective spin vectors. Once the spin vectors are sufficiently separated, the effective loss rate coefficient $K(E, E', t)$ becomes non-negligible and the atom number begins to decay. At $a_S = 5a_0$ ($\zeta = 1.03$), the data are almost indistinguishable from the $a_S = 0a_0$ case, Fig. 4(a). This is consistent with Fig. 2, where, for $a_S = 5a_0$ at our experimental densities, the system is still in the energy-dependent precession-dominated regime. The data show that a transition out of this dynamical phase occurs between $a_S = 5a_0$ and $a_S = 10a_0$ ($\zeta = 2.32$), where the measurements at $a_S = 10a_0$ exhibit the onset of loss suppression, Fig. 4(b). The loss is further suppressed for the $a_S = 15a_0$ ($\zeta = 3.59$) data, Fig. 4(c), and even more for the $a_S = 24a_0$ ($\zeta = 5.39$) data, Fig. 4(d), reflecting the increasing collective alignment of the spins, as depicted for the lossless case of Fig. 2.

Our collective spin vector model of loss for the energy-space lattice is in good quantitative agreement with measurements. The average of the values of K_2^a used to generate the curves in Fig. 4, $62 \pm 6.2 \mu\text{m}^3/\text{s}$, is in good agreement with the predicted value of $69.4 \mu\text{m}^3/\text{s}$ [21]. For extraction of K_2^a from loss measurements in a 50–50 mixture, we assume that a pair of colliding atoms is in the product state $|1\rangle_i|2\rangle_j$ and hence has a probability $|\langle \Psi_a(i, j) | 1\rangle_i | 2\rangle_j \rangle|^2 = 1/2$ to be in the antisymmetric spin state [21]. However, we find that the values of K_2^a used in the model need to be *half* of those extracted from measurements in the 50–50 mixture [21]. This origin of this discrepancy is not yet clear.

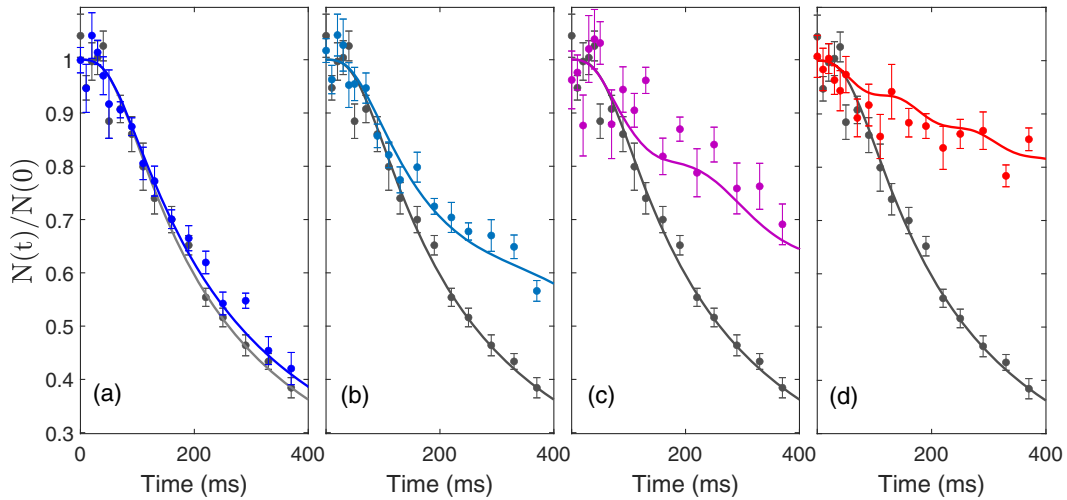


FIG. 4. Suppression of optically induced loss versus illumination time as the scattering length is increased. $N(t)/N(0)$ is the atom fraction remaining after a time t . For reference, the lower black curves show the data and the model for a noninteracting gas $a_S = 0a_0$ ($\zeta = 0$). Each point represents the average of six shots, and the error bar is the standard deviation of the mean. (a) $a_S = 5a_0$ ($\zeta = 1.03$), (b) $a_S = 10a_0$ ($\zeta = 2.32$), (c) $a_S = 15a_0$ ($\zeta = 3.59$), (d) $a_S = 24a_0$ ($\zeta = 5.39$). Note that the interaction strength ζ is not precisely linear in the scattering length due to slight variations in the density. Predictions use half of the two-body loss constant K_2^a measured for each scattering length in a 50–50 mixture, tabulated in [21].

In summary, we have observed dynamical collective suppression of optically induced inelastic scattering in a coherently prepared, weakly interacting Fermi gas. As the scattering length is increased at fixed initial density, we observe a crossover from high to low loss. We understand this suppression via the Pauli principle, where the system undergoes a crossover into a magnetized dynamical phase with parallel collective spin vectors, Fig. 2, causing suppression of s -wave scattering. In this way, loss suppression serves as a new probe of the magnetization of the system. We have developed a loss model that quantitatively agrees with observations and incorporates the many-body evolution of the collective spin vectors. This work paves the way for tailoring of spin-spin couplings by optical control the interactions [21], as the accompanying loss can now be included in energy-space spin-lattice models.

Acknowledgments—Primary support for this research is provided by the Air Force Office of Scientific Research (FA9550-22-1-0329). Additional support is provided by the National Science Foundation Grants No. PHY-2006234 and No. PHY-2307107.

-
- [1] M. Junker, D. Dries, C. Welford, J. Hitchcock, Y. P. Chen, and R. G. Hulet, Photoassociation of a Bose-Einstein condensate near a Feshbach resonance, *Phys. Rev. Lett.* **101**, 060406 (2008).
- [2] S. Lapp, J. Ang'ong'a, F. A. An, and B. Gadway, Engineering tunable local loss in a synthetic lattice of momentum states, *New J. Phys.* **21**, 045006 (2019).
- [3] L. Zhou, H. Li, W. Yi, and X. Cui, Engineering non-Hermitian skin effect with band topology in ultracold gases, *Commun. Phys.* **5**, 252 (2022).
- [4] J. Li, A. K. Harter, J. Liu, L. de Melo, Y. N. Joglekar, and L. Luo, Observation of parity-time symmetry breaking transitions in a dissipative Floquet system of ultracold atoms, *Nat. Commun.* **10**, 855 (2019).
- [5] Z. Ren, D. Liu, E. Zhao, C. He, K. K. Pak, J. Li, and G.-B. Jo, Chiral control of quantum states in non-Hermitian spin-orbit-coupled fermions, *Nat. Phys.* **18**, 385 (2022).
- [6] G. B. Partridge, K. E. Strecker, R. I. Kamar, M. W. Jack, and R. G. Hulet, Molecular probe of pairing in the BEC-BCS crossover, *Phys. Rev. Lett.* **95**, 020404 (2005).
- [7] D. Bauer, M. Lettner, C. Vo, G. Rempe, and S. Dürr, Control of a magnetic Feshbach resonance with laser light, *Nat. Phys.* **5**, 339 (2009).
- [8] H. Wu and J. E. Thomas, Optical control of Feshbach resonances in Fermi gases using molecular dark states, *Phys. Rev. Lett.* **108**, 010401 (2012).
- [9] T. L. Nicholson, S. Blatt, B. J. Bloom, J. R. Williams, J. W. Thomsen, J. Ye, and P. S. Julienne, Optical Feshbach resonances: Field-dressed theory and comparison with experiments, *Phys. Rev. A* **92**, 022709 (2015).
- [10] L. W. Clark, L.-C. Ha, C.-Y. Xu, and C. Chin, Quantum dynamics with spatiotemporal control of interactions in a stable Bose-Einstein condensate, *Phys. Rev. Lett.* **115**, 155301 (2015).
- [11] A. Jagannathan, N. Arunkumar, J. A. Joseph, and J. E. Thomas, Optical control of magnetic Feshbach resonances by closed-channel electromagnetically induced transparency, *Phys. Rev. Lett.* **116**, 075301 (2016).
- [12] X. Du, Y. Zhang, J. Petricka, and J. E. Thomas, Controlling spin current in a trapped Fermi gas, *Phys. Rev. Lett.* **103**, 010401 (2009).
- [13] U. Ebling, A. Eckardt, and M. Lewenstein, Spin segregation via dynamically induced long-range interactions in a system of ultracold fermions, *Phys. Rev. A* **84**, 063607 (2011).
- [14] S. Pegahan, J. Kangara, I. Arakelyan, and J. E. Thomas, Spin-energy correlation in degenerate weakly interacting Fermi gases, *Phys. Rev. A* **99**, 063620 (2019).
- [15] F. Piéchon, J. N. Fuchs, and F. Laloë, Cumulative identical spin rotation effects in collisionless trapped atomic gases, *Phys. Rev. Lett.* **102**, 215301 (2009).
- [16] S. S. Natu and E. J. Mueller, Anomalous spin segregation in a weakly interacting two-component Fermi gas, *Phys. Rev. A* **79**, 051601(R) (2009).
- [17] C. Deutsch, F. Ramirez-Martinez, C. Lacroûte, F. Reinhard, T. Schneider, J. N. Fuchs, F. Piéchon, F. Laloë, J. Reichel, and P. Rosenbusch, Spin self-rephasing and very long coherence times in a trapped atomic ensemble, *Phys. Rev. Lett.* **105**, 020401 (2010).
- [18] S. Smale, P. He, B. A. Olsen, K. G. Jackson, H. Sharum, S. Trotzky, J. Marino, A. M. Rey, and J. H. Thywissen, Observation of a transition between dynamical phases in a quantum degenerate Fermi gas, *Sci. Adv.* **5**, eaax1568 (2019).
- [19] A. P. Koller, M. L. Wall, J. Mundinger, and A. M. Rey, Dynamics of interacting fermions in spin-dependent potentials, *Phys. Rev. Lett.* **117**, 195302 (2016).
- [20] M. L. Wall, Simulating fermions in spin-dependent potentials with spin models on an energy lattice, *Phys. Rev. A* **102**, 023329 (2020).
- [21] C. A. Royse, J. Huang, and J. E. Thomas, companion paper, Many-body suppression of optically induced inelastic scattering in a weakly interacting Fermi gas near a Fano-Feshbach resonance, *Phys. Rev. A* **110**, 023322 (2024).
- [22] J. Huang and J. E. Thomas, Energy-resolved spin correlation measurements: Decoding transverse spin dynamics in weakly interacting Fermi gases, *Phys. Rev. A* **109**, L041301 (2024).
- [23] Y. Margalit, Y.-K. Lu, F. Çağrı Top, and W. Ketterle, Pauli blocking of light scattering in degenerate fermions, *Science* **374**, 976 (2021).
- [24] C. Sanner, L. Sonderhouse, R. B. Hutson, L. Yan, W. R. Milner, and J. Ye, Pauli blocking of atom-light scattering, *Science* **374**, 979 (2021).
- [25] A. B. Deb and N. Kjærgaard, Observation of Pauli blocking in light scattering from quantum degenerate fermions, *Science* **374**, 972 (2021).
- [26] R. Jannin, Y. van der Werf, K. Steinebach, H. L. Bethlem, and K. S. E. Eikema, Pauli blocking of stimulated emission in a degenerate Fermi gas, *Nat. Commun.* **13**, 6479 (2022).
- [27] N. Arunkumar, A. Jagannathan, and J. E. Thomas, Designer spatial control of interactions in ultracold gases, *Phys. Rev. Lett.* **122**, 040405 (2019).

- [28] K. Hazzard and B. Gadway, Synthetic dimensions, *Phys. Today* **76**, No. 4, 62 (2023).
- [29] J. Huang, C. A. Royse, I. Arakelyan, and J. E. Thomas, Verifying a quasiclassical spin model of perturbed quantum rewinding in a Fermi gas, *Phys. Rev. A* **108**, L041304 (2023).
- [30] C. Lhuillier and F. Laloë, Transport properties in a spin polarized gas (I), *J. Phys. (Paris)* **43**, 197 (1982).
- [31] E. P. Bashkin, Spin waves and quantum collective phenomena in Boltzmann gases, *Sov. Phys. Usp.* **29**, 238 (1986).